AIAA JOURNAL
Vol. 37, No. 7, July 1999

Application of Particle Image Velocimetry to a Small-Scale de Laval Nozzle

N. J. Lawson*
University of Melbourne, Melbourne, Victoria 3052, Australia
and
G. J. Page,† N. A. Halliwell,‡ and J. M. Coupland§
Loughborough University, Leicestershire, England LE11 3TU, United Kingdom

The application of particle image velocimetry (PIV) to a Mach 1.4 de Laval expansion nozzle is described. Velocity measurements are taken inside and outside the nozzle and are compared to schlieren data. The PIV technique is shown to resolve a normal shock inside the nozzle and underexpanded shock cell structures outside the nozzle in the open jet with a maximum spatial resolution of 0.54 mm, which is higher than has previously been achieved. A Reynolds-averaged computational fluid dynamics (CFD) simulation is also described and used to provide a priori data for a PIV optimization method previously published by the authors. The instantaneous PIV measurement of the steady normal shock, inside the nozzle, is shown to achieve reasonable agreement with the CFD prediction within experimental limits. Problems encountered at the recording stage with respect to seeding contamination of the viewing area are also highlighted, and a solution using an alternative seeding method is described.

Nomenclature

D = interrogation region length
D_r = dynamic range
d = particle image size
d_p = particle size
E = absolute velocity measurement error
f_n = f number
L = spatial resolution
M = magnification
R_N = interrogation region pixel resolution
V_{max} = maximum fluid velocity in the measurement volume
V_{min} = minimum fluid velocity in the measurement volume
V_1 = minimum velocity in the interrogation region
V_2 = maximum velocity in the interrogation region
W_e = required laser power
Δt = laser pulse separation
δz = depth of field
ε = exposure rating of film
λ = wavelength of laser light
σ_E = autocorrelation random error
φ = spatial velocity gradient strength

Introduction

PARTICLE image velocimetry (PIV) is a well-established nonintrusive technique for recording instantaneous two-dimensional fluid velocity maps from a single plane of interest.[1,2] This makes the technique useful for the validation of computational fluid dynamics (CFD), particularly where sampling times are prohibitively short such as a supersonic blowdown facility. In its simplest form PIV uses double-exposure photography to record the position of seeding particles illuminated by a thin light sheet. Following photographic development, a two-dimensional fluid velocity map is produced using optical or digital spatial autocorrelation analysis to determine the seeding particle displacement within each small region of the flow.[3,4]

Although PIV is well-established, application of the technique to transient high-speed flow regimes has been limited.[5–8] To be viable for CFD code validation, the technique must produce velocity data with acceptable spatial resolution and accuracy. These requirements depend on achieving optimized seeding levels in the flow and by using appropriate seeding particles.[2] The latter requirement has already been comprehensively studied and developed using laser Doppler anemometry.[9]

Achieving optimum seeding levels when making enclosed high-speed flow measurements, however, still presents significant problems. This was demonstrated in previous work[5] when applying PIV to an enclosed turbine cascade. Seeding densities, in this case of approximately one particle pair per interrogation region, were the major limiting factor in restricting spatial resolution, and the data-extraction technique identified the position of individual particle images. This low image density PIV is often termed particle tracking velocimetry (PTV). Work investigating open jet supersonic flows[6–8] has achieved higher seeding densities and consequently has permitted the application of automated correlation data-processing techniques. In these cases seeding densities could be optimized allowing for millimeter scale spatial resolution. Although the previous work has demonstrated the potential for the application of PIV to high-speed flows, further work is still required to extend the technique to any given high-speed flow regime.

In this paper we extend the application of PIV to high-speed flow measurement through investigation of a de Laval expansion nozzle. A CFD model of the nozzle is also described and used as a tool to optimize the PIV experiment and for comparison with the experimental measurement of the steady shock inside the nozzle. This work demonstrates the potential of PIV for both enclosed and open high-speed flow measurement at a scale representative of minimum sizes found in gas turbine environments. The feasibility of the technique is proven, and the practical problems with PIV supersonic flow measurement at this scale are identified.

In the first part a CFD model is introduced for the flow inside the nozzle. Following this, the PIV experimental optimization is completed using CFD data. The PIV rig, recording, and data-processing systems are then described, and finally results from the nozzle are discussed and compared to the schlieren measurement and the CFD prediction.

CFD Modeling

This section outlines a CFD model of the de Laval expansion nozzle, which will be used to provide a priori data required to both optimize the PIV experiment and provide comparison data.

Received 27 April 1998; revision received 10 February 1999; accepted for publication 17 February 1999.

*Research Fellow, The G. K. Williams Cooperative Research Centre, Department of Chemical Engineering.
†Lecturer, Department of Aeronautical and Automotive Engineering.
‡Professor, Department of Mechanical Engineering.
§Senior Lecturer, Department of Mechanical Engineering.

The CFD methodology employed in the present work solves the time-dependent Reynolds-averaged Navier–Stokes (RANS) equation using a control volume formulation and the two-equation k-ε transport model for turbulence closure.[10] For further details of the algorithm see references.[11,12] All calculations have been carried out using a second-order spatial discretization. This turbulence model has been chosen for the current work as it is probably the most widely used and well-understood transport turbulence models. Because this is a wall-bounded flow, no compressibility corrections to the turbulence model are required. (The Morkovin hypothesis is valid up to $M \cong 5$.)

The methodology has been extensively used for a variety of propulsion installation applications, such as the prediction of hot gas ingestion from vertical landing aircraft.[13] Also, the method has been validated for shock-wave/boundary-layer interaction flows by predicting the benchmark solutions for the Bachalo and Johnson[14] axisymmetric bump, as presented by Bardina et al.[15]

Because the nozzle is symmetrical about the centerline, only half of the experimental domain was modeled. The parametric definition of the nozzle geometry was calculated by using measurements of the internal nozzle profile and a cubic spline fit routine. This was then used to generate a mesh with 150 cells in the streamwise direction and 40 cells normal to the flow. Clustering of cells normal to the wall was used to resolve the boundary layer. Uniform streamwise spacing was employed with the number of streamwise cells ensuring a shock wave could be adequately resolved at any position in the nozzle. The mesh dimensions and spacing were based upon the second author's experience of computing shock-wave/boundary-layer interaction flows as reported in Ref. 16. For this flow the resulting grid resolved the boundary layer upstream of the shock with approximately 10 points. The use of wall functions to bridge the near wall region meant that this number of points gives a good reproduction of the boundary-layer profile; the y^+ value of the points adjacent to the wall varied between 20 and 30.

The inlet condition imposed total pressure and temperature whereas the outlet boundary imposed a static pressure constraint, the total and static values being those measured in the experiment. The inlet values for the turbulence model were based upon an assumed 3% turbulence intensity and a length scale of one-third of the total duct height. In this type of flow, the production of turbulence energy in the boundary layer and shock interaction region is large, and the overall solution is only weakly sensitive to the chosen turbulence model values at the inlet.[16]

In the following section some information about the flowfield predicted by the CFD model will be used to optimize the PIV system; comparisons will be made between the CFD predictions and PIV measurements in the results section.

Particle Image Velocimetry: Experiment Optimization

The following outlines the application of CFD data to optimize the PIV experiment and also to allow estimates of error in the PIV data.

Experimental Optimization

Lawson et al.[17] have described an optimization method for a double-pulsed PIV experiment based on autocorrelation analysis. They have shown that in order to retrieve a valid velocity vector from an interrogation region there exists a strong interdependence between the dynamic range D_r of the flow defined by

$$D_r = \frac{|V_{\max}|}{|V_{\min}|} \tag{1}$$

where $|V_{\max}|$ and $|V_{\min}|$ are the maximum and minimum velocities measured in the flow plane and the velocity gradient strength φ defined by

$$\varphi = \frac{|V_2 - V_1|}{|V_{\max}|} \tag{2}$$

Here, $|V_2 - V_1|$ is the velocity change across the interrogation region. A high dynamic range requirement necessarily restricts the strength of the velocity gradient in a chosen region and vice versa. The latter condition is crucial to the design of a PIV experiment for use in supersonic flows.

Table 1 CFD optimization data

Variable	Value
Dynamic range D_r	2
Maximum velocity gradient ϕ, %	
1) Outside shock region	5
2) Inside shock region	40
Maximum fluid velocity $V_{\max}$, m/s	410

Table 2 Experimental data

Variable	Value
System magnification M	0.67
Particle image size d, μm	17
Required spatial resolution L, mm	0.5
Minimum seeding level, particle image pairs per region	12

Table 3 Random error estimates

Interrogation region resolution R_N, pixels	σ_E, % of full scale (inside shock region $\phi = 40\%$)	σ_E, % of full scale (outside shock region $\phi = 5\%$)
32 × 32	1.42	1.24
64 × 64	1.07	0.60
128 × 128	0.85	0.48
256 × 256	0.76	0.40

With a priori knowledge of D_r, φ, and $|V_{\max}|$, it is possible to use the method to determine a laser pulse separation Δt for a PIV experiment, which will ensure that, on average, from a series of experiments at least 50% of valid vectors will be obtained from a worst-case interrogation region in the flow. The experiments are then defined as being optimized. The CFD predictions used to provide the a priori knowledge are listed in Table 1.

This data are used with the experimental parameters listed in Table 2 to calculate the laser pulse separation Δt for the experiment. The system magnification M is defined in terms of the ratio of object and image distances and is that which is required to capture the flow area. The spatial resolution of the system is defined by

$$L = D/M \tag{3}$$

where D is the interrogation region length and the particle image size d is dependent on the depth of field and laser power of the system.

From the data provided in Tables 1 and 2, the optimization method[17] is used to calculate a laser pulse separation of $\Delta t = 245$ ns, equivalent to a particle image displacement of 30% of the interrogation region length D. With this pulse separation the experiment is optimized up to a maximum allowable dynamic range D_r and velocity gradient strength φ of 3.8 and 75%, respectively. These values are therefore well in excess of those predicted for the worst case by the CFD model, i.e., $D_r = 2$ and $\varphi = 40\%$ as shown for inside the shock region in Table 1. This means the PIV experiment will have sufficient performance to ensure a minimum of 50% of valid vectors, on average, inside this region where the velocity gradients and dynamic range are highest.

Data-Processing Error Analysis

Estimation of measurement accuracy for spatial autocorrelation processing in PIV experiments using a Monte Carlo simulation has been investigated by Lawson et al.[18] This work has shown that a random error is necessarily present and depends upon the velocity gradient strength, dynamic range, and the interrogation region pixel resolution used in the data processing. The error is caused by the random distribution of particle image positions within the interrogation region and perturbations in the correlation signal peak position because of local noise peaks. Table 3 lists the random error σ_E predictions from the Monte Carlo simulation as a percentage of the maximum measurable velocity.

Table 4 Absolute error estimates, $R_N = 256$

Particle image displacement, % of D	E, % (inside shock region $\phi = 40\%$)	E, % (outside shock region $\phi = 5\%$)
15	5.1	2.7
30	2.5	1.3

These estimates show that the best accuracy will be achieved by using an interrogation region resolution of $R_N = 256$, which agrees with previous work by Prasad et al.[19] Therefore all of the following results are processed using this interrogation region resolution. Table 4 lists the range of absolute measurement error E predicted for $R_N = 256$ and the displacement restriction of 30% of D.

These results show a maximum error in measurement of 5.1% is predicted in the shock region of the flow. The majority of the data points, however, would be expected to have absolute errors of between 1.3 and 2.7% across the measurement range, which is acceptable for the flow under investigation. The higher error in the shock region, however, should still allow detection of a normal shock in flow. These error figures compare well with previous estimates of PIV measurement error.[20]

Practical Considerations

In PIV experimental design there are a number of variables that can be adjusted to suit the nature of the recorded flow. The following section outlines calculations used to design the experimental setup.

Particle Tracer Requirements

A suitable particle must sufficiently follow the strongest velocity gradients encountered in the flow. Previous work has recommended the seeding size be based on particle Stokes number.[21,22] Therefore, assuming the normal shock to be equivalent to a step change in velocity and to be the most severe velocity gradient in the flow, for the variables outlined in Table 1 a particle size of $d_p = 0.5\ \mu$m will ensure 99% speed recovery 1 mm after the shock.[21]

Optical Considerations

The photographic recording system allows adjustment of the depth of field and particle image diameter. The depth of field is normally matched to the light sheet thickness, which is dictated by the out-of-plane nature of the fluid flow being measured. Here, for the required flow measurement area of approximately 50 × 40 mm this corresponds to a system magnification of $M = 0.67$ for the system chosen. Therefore from recommended formulas,[2] when using Nd:YAG laser light at $\lambda = 532$ nm and with an f number range of $f_n = 2$–16, the depth of field available from the system will be $\delta z = 0.024$–1.5 mm. With a particle diameter of $d_p = 0.5\ \mu$m, this results in a diffraction limited particle image diameter of between $d = 4.3$–$35\ \mu$m for the corresponding f number range of $f_n = 2$–16 (Ref. 2). These depths of field, particle image size, and f number ranges now allow the film characteristics and laser power W_e to be specified.

Film and Laser Requirements

Kodak Technical Pan film[23] has the required noise and contrast characteristics for PIV and with a resolution of 150 line pairs/mm allows the minimum particle image size of $d = 4.3\ \mu$m to be recorded. Previous formulas have shown[2] that an estimate of the required laser power for sufficient exposure can be made from the light sheet and optical settings of the system providing an exposure rating of the film is known. Therefore using Kodak Technical Pan film with a typical exposure rating ϵ of 1 mJ/m2 corresponding to 125 ASA and Nd:YAG laser light with $\lambda = 532$ nm, Table 5 lists the range of laser powers required to expose the flow area.

Because the available laser power in this case was limited to 150 mJ per pulse, it can be seen from Table 5 that the f number of the recording must be restricted. Choice of an f number of $f_n = 8$, which corresponds to a particle image size of $d = 17\ \mu$m and a depth of field of $\delta z = 0.4$ mm, was found to be sufficient for the PIV measurements.

Table 5 Laser power requirements

Depth of field $\delta z D$, mm	f number f_n	Particle image size d, μm	Required laser power W_e, mJ
0.024	2	4.3	7.2×10^{-4}
1.5	16	35	220

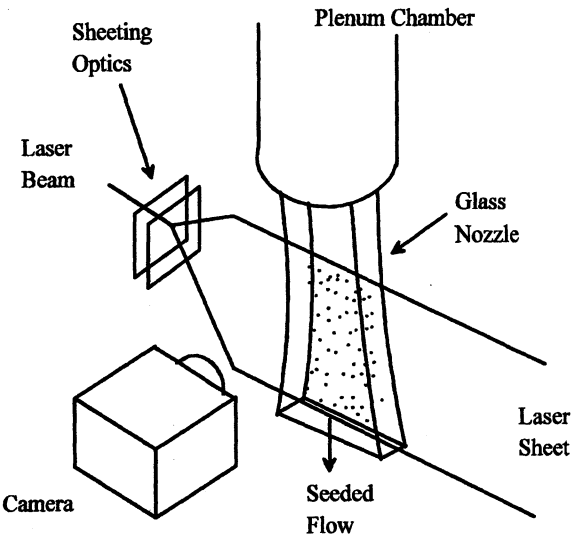

Fig. 1 Nozzle/plenum chamber configuration.

Rig Design/Experimental Setup

A de Laval expansion nozzle design was chosen to allow a simple, enclosed supersonic flow regime to be studied at a scale representative of gas turbine environments.[24] This type of nozzle also allows study of the open exhaust jet, which provides a more complex supersonic flow structure for comparison with the internal nozzle flow. In what follows we describe the design and implementation of the PIV setup in more detail.

Figure 1 illustrates the setup used for the recording stage. The nozzle design was a scaled down version of a Plint and Partners Mach 1.4 supersonic wind tunnel and consisted of a rectangular section de Laval expansion nozzle with a throat size of 10 mm square. For optical access an all-glass design was constructed by sandwiching two identical preformed sides between two glass plates, which were cemented together. The shape of the sides was accurately produced by shaping glass strips at 800°C over a high-temperature ceramic former. The nozzle was then clamped down to a plenum chamber design consisting of a high-pressure cylinder of diameter 200 mm and height 500 mm with an air line feed and nozzle inlet at opposite ends containing a converging exit in the form of a V-type slot. This gave a combined plenum exit to throat contraction ratio of 30:1. The flow was seeded by direct injection into the plenum chamber, where after mixing it would pass through the nozzle. Figure 2 illustrates a typical open-jet PIV transparency.

For measurements inside the nozzle, seeding the entire plenum chamber was found to cause significant problems with particles coating the nozzle walls. Coagulation of the particles rapidly formed droplets, which moved up the walls causing aberration of the particle images. Therefore an alternative seeding system was required. The new design consisted of a seeding plenum chamber within the main plenum chamber, incorporating a 3-mm diam injector tube centrally protruding into the glass nozzle to a point 30 mm upstream of the throat, as illustrated in Fig. 3. Central injection was found to sufficiently reduce wall coating to allow several PIV pictures to be taken before the nozzle required cleaning, although the whole flowfield could not now be investigated. Figure 4 illustrates a typical PIV transparency with central seeding injection.

A commercially available Technical Solutions, Inc., six-jet atomizer was used to seed the flow by injection under pressure into the plenum chamber. By choosing one to six jets on the seeder, seeding

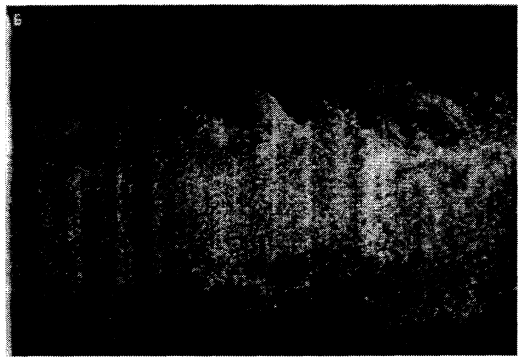

Fig. 2 Typical PIV transparency taken from the open-jet flow.

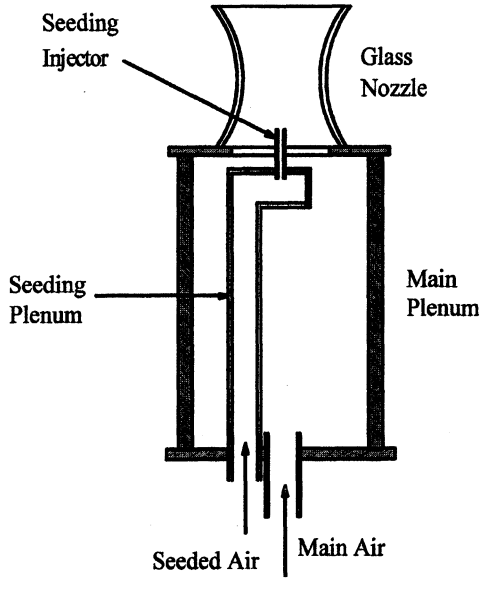

Fig. 3 Seeding injector design.

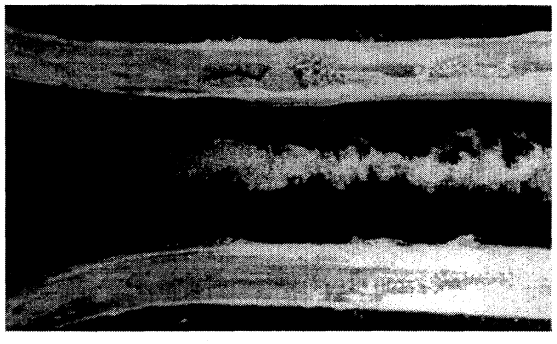

Fig. 4 PIV transparency taken from inside the nozzle with central seeding injection.

densities could be easily adjusted. To obtain the recommended submicron seeding size range, OLNA DS15 mineral oil was used in the seeder.[25]

The recording system consisted of a 35-mm Nikon F3 camera with a 105-mm Micro-Nikor lens and a Spectra Physics double-pulsed Nd:YAG laser giving output light of 150 mJ per pulse with a 10-ns duration and a wavelength of $\lambda = 532$ nm. Pulse separations of 150 ns to infinity were possible with the driver circuits used. Also a Nikon DW-4 12x eyepiece was fitted to aid focusing and alignment of the camera relative to the light sheet.

Data processing was carried out using the autocorrelation software Visiflow by AEA Technology, Ltd.[26] A pixel resolution of 256 x 256 was chosen with a 60% overlap to provide the necessary accuracy and a spatial resolution of 0.54 mm. Transparency processing time was 45 min to yield 800 data points, which were validated by using a velocity range determined from the CFD simulation. Any missing data points were then interpolated and smoothed as outlined by previous workers.[27] In addition to the PIV analysis, schlieren results were recorded from the nozzle and open jet to define shock locations and geometry. An 8-ms exposure was used for these pictures.

Results

The following section presents PIV results obtained from the open jet and nozzle. The practical problems involved with flow measurements from the nozzle are discussed.

Nozzle Results

Figure 5 shows the original PIV data obtained from inside the nozzle with central seeding injection and a stagnation plenum pressure and temperature of $P_0 = 162.0$ kPa and $T_0 = 288$ K, respectively, where the x and y axes origins are located at the plenum chamber top and nozzle centerline, respectively. The vector map covers approximately 25% of the total cross-sectional area of the nozzle. A global mean of 200 m/s has been subtracted from the vectors to aid shock location. The exploded view of the vector map illustrates the shock area, which can be seen from the change in vector magnitude. This result shows that PIV can resolve the shock across one interrogation region length L, which is 0.54 mm wide. Gaps in the central areas of the vector map are caused by poor mixing of the seeding and window contamination, which causes particle image aberrations. These effects result in a reduction of autocorrelation signal-to-noise ratio, which results in an invalid measurement.[17]

An illustration of typical window contamination is shown in Fig. 6, where it can be seen in the center section of the nozzle. This picture is a schlieren photograph of the nozzle with the normal shock clearly visible in the center of the picture. Previous work[5] has avoided window contamination by using a short duration blowdown facility and low seeding densities. The low seeding density, however, restricts the spatial resolution possible to around 2 mm/point with 200 vector points/map. In this case the spatial resolution is around 0.5 mm/point with between 600–800 vector points. This improvement is because of the increased seeding levels, which were achieved in the rig, but is also at the cost of significant window contamination. An alternative method that could be used to reduce window contamination involves a pulsed seeding system as demonstrated by Molezzi and Dutton,[7] which, unfortunately, was not available for these measurements.

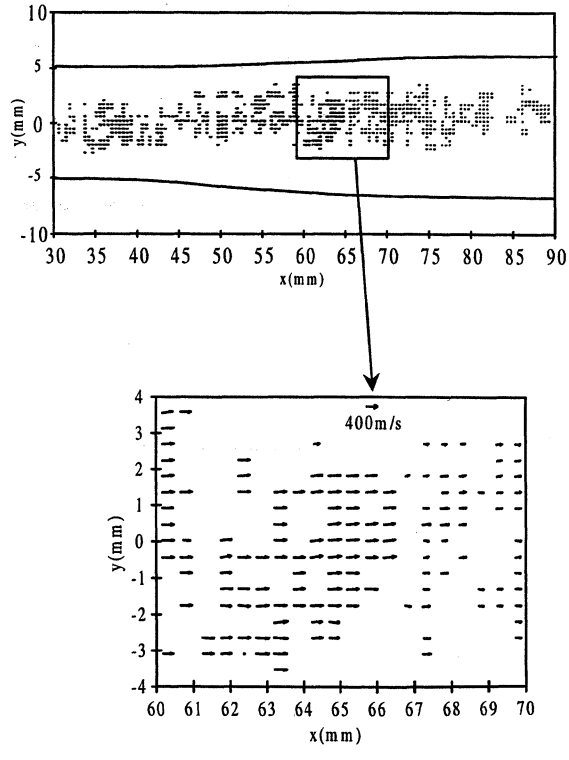

Fig. 5 PIV vector plot from the nozzle showing a normal shock position.

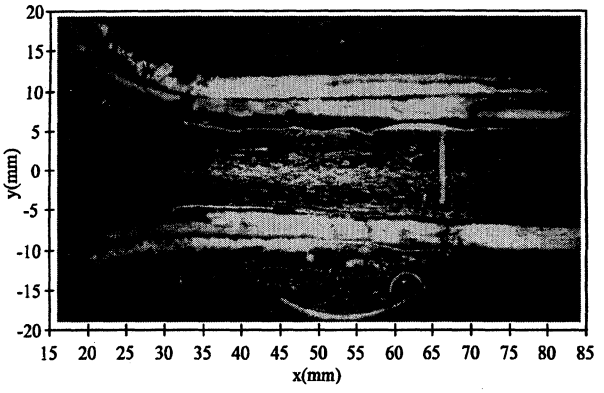

Fig. 6 Schlieren photograph showing a normal shock inside the nozzle.

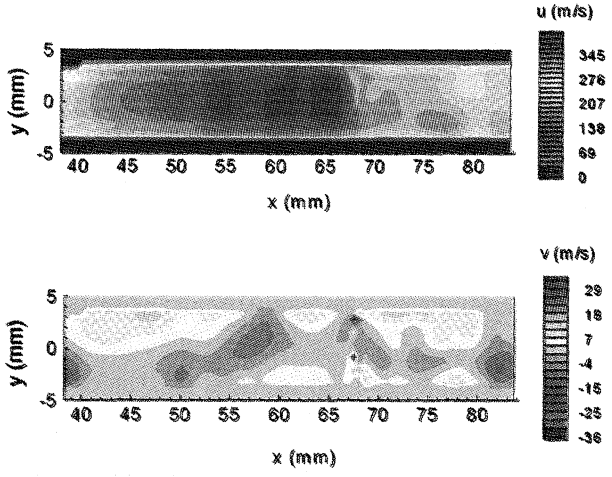

Fig. 7 Streamwise u and normal v components of velocity inside the nozzle: spatial resolution $L = 0.54$ mm.

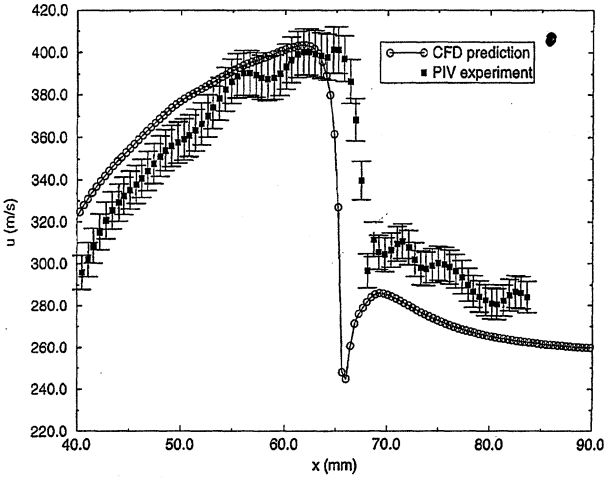

Fig. 8 Streamwise u centerline velocity profile inside the nozzle: comparison with CFD prediction.

Figure 7 shows the interpolated and smoothed streamwise u and normal v components of velocity inside the nozzle for a stagnation plenum pressure conditions of $P_0 = 162.0$ kPa at a spatial resolution of $L = 0.54$ mm. The shock position recorded from the schlieren results agrees to within 3 mm. The discrepancy in position is attributed to pressure fluctuations in the air supply, which was not completely stabilized. The v component is less than 10% of the u component and does not significantly change across the shock, which would be expected because of the one-dimensional nature of the flow in this type of nozzle geometry.

Figure 8 shows a comparison of the streamwise u velocity along the nozzle centerline for the CFD predictions and the PIV measurements. Care must be taken when comparing CFD results, which solve the ensemble-averaged equations for the mean flow, with the instantaneous snapshot of the flowfield provided by the PIV methodology. Along the nozzle centerline turbulent fluctuations are small, and the unsteadiness is likely to be dominated by fluctuations in the position of the shock wave, which is sensitive to small pressure fluctuations in the experimental rig. It is reasonable to compare the two types of information if the possibility of small shock movements is taken into account.

Comparing shock locations, the PIV measurement indicates the shock to be 2 mm downstream of the CFD prediction. This is within the shock positional error of 3 mm indicated by comparing the PIV measurements with schlieren photography. Immediately upstream of the shock, agreement is within the experimental error bounds, and in particular the peak velocity ahead of the shock is in excellent agreement. Near the entrance of the nozzle, the PIV measurements show consistently lower velocities than the predictions. At a given station the CFD prediction is in close agreement with the velocity calculated by a quasi-one-dimensional analysis. It would appear likely that in the experimental setup the junction between the plenum chamber and the nozzle inlet had an insufficient radius, resulting in higher velocities at the corners, and consequently a depression of centerline velocity in the initial portion of the inlet. At the base of the shock, the CFD predicts a velocity consistent with normal shock theory, followed by a rapid expansion as the shock wave causes the boundary layer to thicken and lead to an effective reduction in area for the effectively inviscid core flow. The PIV measurements fail to resolve the correct velocity at the base of the shock; this is likely to be caused by the failure of the seeding particles to follow accurately the severe deceleration in the extremely thin shock wave, followed by a sudden acceleration. The PIV measurements in the downstream region show higher velocities than the predictions, indicating that a stronger shock-wave/boundary-layer interaction has occurred in the measurements with greater boundary-layer thickening (and possibly a separated flow zone). It is a common flaw with current turbulence models, and the k-ε model in particular, that the boundary-layer thickening and possible separation are under-predicted.[15,16]

Another feature present in the measurements is several spurious troughs and peaks in velocity. Upstream of the shock these variations can be attributed to oblique expansion and compression waves travelling across the nozzle; these waves emanate from surface discontinuities created by the nozzle manufacturing process. Downstream of the shock, where the flow is subsonic, this mechanism cannot occur. A second physical explanation is that the likely oscillations of the shock-wave position create a train of perturbations in pressure that travel down the center of the nozzle, resulting in the velocity fluctuations.

Overall, although the agreement between the prediction and measurement is reasonable, the discrepancies can be accounted for by limitations of the measurement methodology, rig design, and CFD modeling.

Open-Jet Results

Figure 9 shows the original PIV data obtained from the open jet with a stagnation plenum pressure of $P_0 = 286.0$ kPa and a spatial resolution of $L = 0.6$ mm where the x and y axes origins are located at the nozzle exit and centerline, respectively. A mean velocity of 400 m/s has been subtracted in the magnified view to aid shock cell location. The vector map covers approximately 80% of the total cross-sectional area of the jet. The remainder of the imaging area could not be processed because of data dropout from low seeding density and high velocity gradients. The area adjacent to the nozzle exit could also not be processed because of excess flare off the rig surface. This resulted in a gap of approximately 5 mm in data adjacent to the exit.

The results in Fig. 9 show that the open-jet results have significantly greater data quantity in comparison with the internal nozzle. These improvements were possible because of the absence of window contamination. This allowed the seeding density to be increased to obtain an improved imaging area to record the full width of the jet. For example, the internal results contained around 800 vector points per map whereas this was increased for the open-jet results to around

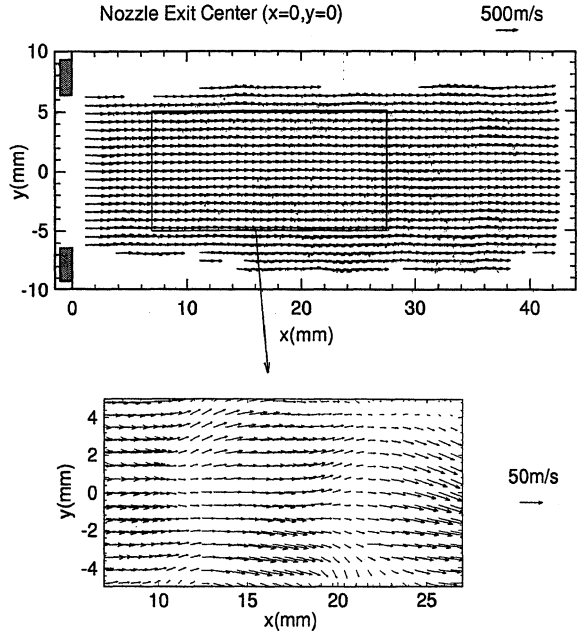

Fig. 9 PIV vector plot from the open jet.

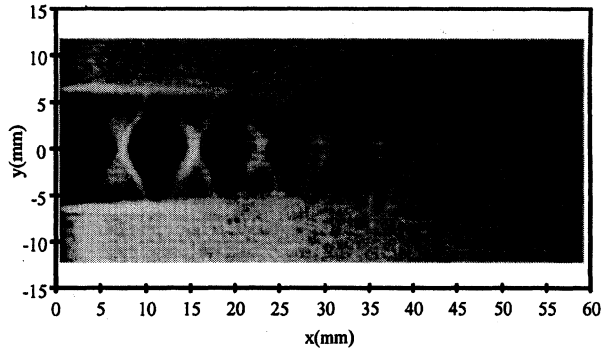

Fig. 10 Schlieren photograph showing a shock cell structure from the open jet.

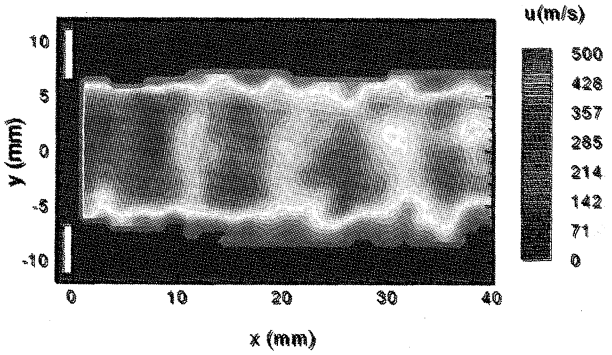

Fig. 11 Streamwise u component of velocity of the open jet: spatial resolution $L = 0.6$ mm.

3000–4000 vector points/map. The spatial resolution attained in this case of 0.6 mm/point is considerably greater than previous open-jet work,[5,6] which achieved a spatial resolution of 1–2 mm/point, respectively.

Figure 10 shows a schlieren image of the open jet at a plenum chamber pressure of $P_0 = 286.0$ kPa. These results show that a shock cell structure exists with the shape of the nozzle flow at the exit indicating an underexpanded jet regime. These flow structures can also be clearly seen as a result in Fig. 11, which illustrates the streamwise u component of the jet for the same plenum pressure. Figure 12, which shows the u centerline velocity profiles at the same

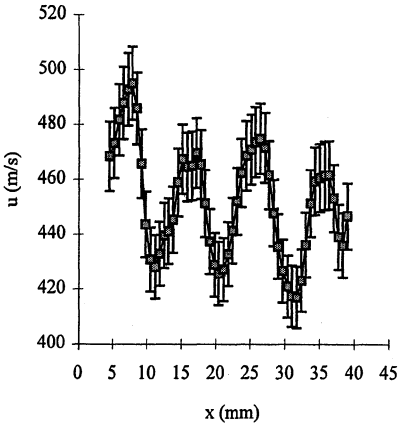

Fig. 12 Streamwise u component centerline velocity profile for the open jet: error bars correspond to $u \pm 2.7\%$.

plenum pressure, also reinforces this result, where it can be seen that a decaying wave train is present in the jet.

Conclusions

The PIV technique has been successfully applied to a de Laval expansion nozzle representative of a scale that would be encountered in a gas turbine environment. Instantaneous velocity data have been obtained from a central plane in the nozzle and the open exhaust jet. Inside the nozzle seeding limitations reduced the vector map to 25% of the cross-sectional nozzle area, but location of a normal shock was still possible to an accuracy of one interrogation region (0.54 mm). The open-jet vector maps characterized the majority of the core fluid flow and allowed shock cells structures to be resolved up to four nozzle widths from the exit and with a scale of less than 10 mm.

A priori flow data from the CFD have allowed application of a technique previously proposed by Lawson et al.[17] to be used to optimize the PIV experiment. The maximum spatial resolution achieved inside the nozzle was 0.54 mm, therefore giving a significant improvement over previously enclosed high-speed work. Error analysis also proved the technique to have sufficient accuracy to resolve shock cell structures both inside and outside the nozzle. This was confirmed from analysis of the vector maps where these structures were visible as a normal shock wave inside the nozzle and a set of shock cells in the open jet.

Inside the nozzle seeding levels of at least 12 particles images per interrogation region recommended by the optimization method were achieved. The high mass flows involved in running the supersonic rig, however, caused significant window contamination when seeding the complete nozzle. Injecting the seeding into the center of the flow reduced this problem but limited the area that could be mapped. Further work is continuing to reduce window contamination problems to allow full-field PIV analysis at this scale.

The limitations of seeding the enclosed flow in terms of window contamination were highlighted when analyzing the open jet from the same nozzle. In this case seeding densities were significantly increased across the complete flowfield without adversely affecting the PIV imaging. This resulted in five times as many vectors per image as the enclosed flow, thus allowing four shock cell flow structures to be observed in the results.

Agreement between CFD predictions and PIV measurements for the nozzle centerline streamwise velocity was reasonable, and the discrepancies could be attributed to identifiable limitations of the measurement technique, rig design, and computational modeling.

Acknowledgments

The authors would like to acknowledge the financial support of Rolls–Royce, plc., and the U.K. Engineering and Physical Sciences Research Council (Award 91593343). The authors would also like to thank John Hancox and the members of the technical staff in the Rolls–Royce Applied Science Laboratories for their advice and guidance during the project.

References

[1]Pickering, C. J. D., and Halliwell, N. A., "Particle Image Velocimetry: A New Field Measurement Technique," *Optical Measurements in Fluid Dynamics*, Inst. of Physics Conf., Series 77, Session 4, Adam Hilger, Bristol, England, UK, 1985, pp. 147–152.

[2]Adrian, R. J., "Particle-Imaging Techniques for Experimental Fluid Mechanics," *Annual Review of Fluid Mechanics*, Vol. 23, 1991, pp. 261–304.

[3]Coupland, J. M., and Halliwell, N. A., "Particle Image Velocity: Rapid Transparency Analysis Using Optical Correlation," *Applied Optics*, Vol. 27, No. 10, 1988, pp. 1919–1921.

[4]Halliwell, N. A., and Pickering, C. J. D., "Analysis Methods in Laser Speckle Photography and Particle Image Velocity," *Interferogram Analysis*, edited by D. W. Robinson and G. T. Reid, Inst. of Physics Publishing, Ltd., Bristol, England, UK, 1993, Chap. 6.

[5]Bryanston-Cross, P. J., Towers, C. E., Judge, T. R., Towers, D. P., Harasgama, S. P., and Hopwood, S. T., "The Application of Particle Image Velocimetry (PIV) in a Short-Duration Transonic Annular Turbine Cascade," *Transactions of the ASME*, Vol. 114, No. 3, 1992, pp. 504–509.

[6]Hocker, R., and Kompenhans, J., "Application of Particle Image Velocimetry to Transonic Flows," *Proceedings of the 5th International Symposium on the Applications of Laser Techniques to Fluid Mechanics and Workshop on the Use of Computers in Flow Measurement*, Springer–Verlag, Berlin, 1990, pp. 415–434.

[7]Molezzi, M. J., and Dutton, J. C., "Application of Particle Image Velocimetry in High Speed Separated Flows," *AIAA Journal*, Vol. 31, No. 3, 1993, pp. 438–446.

[8]Krothapalli, A., Wishart, D. P., and Lourenco, L. M., "Near Field Structure of a Supersonic Jet: 'On Line' PIV Study," *Proceedings of the 7th International Symposium of the Applications of Laser Techniques to Fluid Mechanics*, Springer–Verlag, Berlin, 1994, pp. 26.5.1–26.5.6.

[9]Durst, F., Melling, A., and Whitelaw, J. M., *Principles and Practice of Laser Doppler Anemometry*, Academic, London, 1981, Chap. 10.

[10]Jones, W. P., and Launder, B. E., "The Prediction of Laminarisation with a Two-Equation Model of Turbulence," *International Journal of Heat and Mass Transfer*, Vol. 15, No. 2, 1972, pp. 301–314.

[11]McGuirk, J. J., and Page, G. J., "Total Pressure Loss and Drag Predictions for a Supersonic Circular Pitot Intake," *1993 European Forum—Recent Developments and Applications in Aeronautical CFD*, Royal Aeronautical Society, Bristol, England, UK, 1993, pp. 28.1–28.11.

[12]Page, G. J., Zhao, H., and McGuirk, J. J., "A Parallel Multiblock Reynolds Averaged Navier–Stokes Method for Propulsion Installation Applications," *XII International Symposium on Air Breathing Engines*, AIAA, Reston, VA, 1995, pp. 864–874.

[13]Page, G. J., McGuirk, J. J., Jiang, D., Harper, L. R., and Penrose, C. J., "Application of Computational Fluid Dynamics to Hot Gas Ingestion Modelling," *International Powered Lift Conference*, Royal Aeronautical Society, London, 1998, pp. 23.1–23.11.

[14]Bachalo, W. D., and Johnson, D. A., "Transonic Turbulent Boundary-Layer Separation Generated on an Axisymmetric Flow Model," *AIAA Journal*, Vol. 24, No. 3, 1986, pp. 437–443.

[15]Bardina, J. E., Huang, P. G., and Coakley, T. J., "Turbulence Modeling, Validation, Testing, and Development," NASA TM 110446, April 1997.

[16]Haase, W., Bradsma, F., Elsholz, E., Leschziner, M., and Schwamborn, D., "'EUROVAL'—A European Initiative on Validation of CFD Codes," *Notes on Numerical Fluid Mechanics*, Vol. 42, Friedr. Vieweg and Sohn Verlagsgesellschaft mbH, Braunschweig, Germany, 1993, pp. 185–204.

[17]Lawson, N. J., Coupland, J. M., and Halliwell, N. A., "A Generalised Optimisation Method for Double Pulsed Image Velocimetry," *Optics and Lasers in Engineering*, Vol. 27, No. 6, 1997, pp. 637–656.

[18]Lawson, N. J., "The Application of Particle Image Velocimetry to High Speed Flows," Ph.D. Dissertation, Dept. of Mechanical Engineering, Loughborough Univ., Loughborough, England, UK, 1995.

[19]Prasad, A. K., Adrian, R. J., Landreth, C. C., and Offutt, P. W., "Effect of Resolution on the Speed and Accuracy of Particle Image Velocimetry Interrogation," *Experiments in Fluids*, Vol. 13, No. 2–3, 1992, pp. 105–116.

[20]Keane, R. D., and Adrian, R. J., "Optimisation of Particle Image Velocimeters. Part I: Double Pulsed Systems," *Measurement Science Technology*, Vol. 1, No. 11, 1990, pp. 1202–1215.

[21]Dring, R. P., "Sizing Criteria for Laser Anemometry Particles," *Journal of Fluids Engineering*, Vol. 104, 1982, pp. 15–17.

[22]Samimy, M., and Lele, S. K., "Motion of Particles with Inertia in a Compressible Free Shear Layer," *Physics of Fluids A*, Vol. 3, No. 8, 1991, pp. 1915–1923.

[23]"Kodak Technical Pan Film," Kodak Publication P-255(H), Hemel Hempstead, England, UK, 1993.

[24]Cohen, H., Rogers, G. F. C., and Saravanamuttoo, H. I. H., *Gas Turbine Theory*, 2nd ed., Longman, Harlow, UK, 1972, pp. 117–158.

[25]"Model 9306 TSI Six Jet Atomiser," Users' Manual, TSI, Inc., Fort Myers, FL, 1992, pp. 12–16.

[26]"Visiflow: Software for PIV Analysis. User Guide and Technical Reference," Rev. 9, AEA Technology, Harwell, England, UK, 1997.

[27]Landreth, C. C., and Adrian, R. J., "Measurement and Refinement of Velocity Data Using High Image Density Analysis in Particle Image Velocimetry," *Proceedings of the 4th International Symposium on the Applications of Laser Anemometry to Fluid Mechanics*, Springer–Verlag, Berlin, 1988, pp. 491–497.

J. P. Gore
Associate Editor

Color reproductions courtesy of Loughborough University.